



A Journal of the Gesellschaft Deutscher Chemiker

# Angewandte Chemie

GDCh

International Edition

www.angewandte.org

## Accepted Article

**Title:** Photo-excited oxygen reduction and oxygen evolution reactions enabling a high-performance Zn-air battery

**Authors:** Dongfeng Du, Shuo Zhao, Zhuo Zhu, Fujun Li, and Jun Chen

This manuscript has been accepted after peer review and appears as an Accepted Article online prior to editing, proofing, and formal publication of the final Version of Record (VoR). This work is currently citable by using the Digital Object Identifier (DOI) given below. The VoR will be published online in Early View as soon as possible and may be different to this Accepted Article as a result of editing. Readers should obtain the VoR from the journal website shown below when it is published to ensure accuracy of information. The authors are responsible for the content of this Accepted Article.

**To be cited as:** *Angew. Chem. Int. Ed.* 10.1002/anie.202005929

**Link to VoR:** <https://doi.org/10.1002/anie.202005929>

# Photo-excited oxygen reduction and oxygen evolution reactions enabling a high-performance Zn-air battery

Dongfeng Du, Shuo Zhao, Zhuo Zhu, Fujun Li,\* Jun Chen

**Abstract:** Harvesting solar energy in battery systems is pivotal for a sustainable society and faced with challenges. Herein, a photo-involved Zn-air battery is constructed with two cathodes of poly(1,4-di(2-thienyl))benzene (PDTB) and TiO<sub>2</sub> grown on carbon papers to sandwich a Zn anode. The PDTB cathode is illuminated in a discharging process, where photoelectrons are excited into the conduction band of PDTB to promote oxygen reduction reaction (ORR) and raise the output voltage. In a reverse process, holes in the valence band of the illuminated TiO<sub>2</sub> cathode are driven for oxygen evolution reaction (OER) by an applied voltage. A record-high discharge voltage of 1.90 V and an unprecedented low charge voltage of 0.59 V are achieved in the photo-involved Zn-air battery, regardless of the equilibrium voltage. This work offers an innovative pathway for photo-energy utilization in rechargeable batteries.

Rechargeable Zn-air batteries are promising for their low cost, high safety, and large theoretical energy density of 1086 Wh kg<sup>-1</sup>.<sup>[1]</sup> They operate with an equilibrium voltage of 1.64 V based on the battery reaction of  $2\text{Zn} + \text{O}_2 \leftrightarrow 2\text{ZnO}$ ,<sup>[1b,2]</sup> while the practical discharge voltage is lower than 1.2 V and the high charge voltage is > 2.0 V, which lead to low energy efficiency of < 60%. This is closely related to the slow kinetics of oxygen reduction reaction (ORR) and oxygen evolution reaction (OER) of air cathodes, passivation and dendrite growth of Zn anodes, and hydrogen evolution.<sup>[3]</sup> Substantial efforts have been devoted to active electrocatalysts, electrode protection, and electrolyte formulation, however large discharge/charge voltage gaps above 0.8 V remain.<sup>[3b,4]</sup> It seems that intrinsic changes in the electrode reactions of Zn-air batteries are crucial for reduction of overpotentials in both discharge and charge.

Photo-energy has been utilized in various electrochemical devices for improved reaction kinetics and lowered overpotentials,<sup>[5]</sup> like hydrogen and oxygen evolution and pollutant degradation, etc. It usually involves a semiconductor<sup>[6]</sup> that, upon illumination, generates excited electrons and holes of certain energy levels for electrocatalytic hydrogen evolution reaction and OER, respectively. Recently, light was used to excite electrons in semiconducting polyterthiophene<sup>[7]</sup> and carbon nitride<sup>[8]</sup> to boost the reduction potentials of ORR. This is a promising option to achieve high output voltages in oxygen reduction based electrochemical devices.<sup>[9]</sup> At the same time, BiVO<sub>4</sub> and  $\alpha\text{-Fe}_2\text{O}_3$ <sup>[10]</sup> were attempted under illumination to improve OER and reduce the charge voltage of Zn-air batteries by 0.5-0.8 V. However, the photo-involved reaction is limited by the interfacial resistance of semiconductor and electrolyte, and

the comparability of charge carrier life in semiconductors and the electrochemical reaction kinetics. Up to now, it functions only in ORR or OER of Zn-air batteries. Full utilization of light in both the discharging and charging processes of Zn-air batteries for additional photo-energy conversion is challenging.

Herein, a Zn-air battery with poly(1,4-di(2-thienyl))benzene (PDTB) and titanium dioxide (TiO<sub>2</sub>) as cathodes in the respective discharging and charging process, which can capture light separately for ORR and OER, is demonstrated. They are *in situ* formed on carbon fibers of carbon papers to promote the cathode reactions under illumination. These enable a record-high discharge voltage of 1.90 V and an unprecedented low charge voltage of 0.59 V in the Zn-air battery, which are realized by the photo-excited ORR and OER in the discharging and charging process, respectively. This would be a promising strategy for high energy efficiency of Zn-air batteries and beyond.

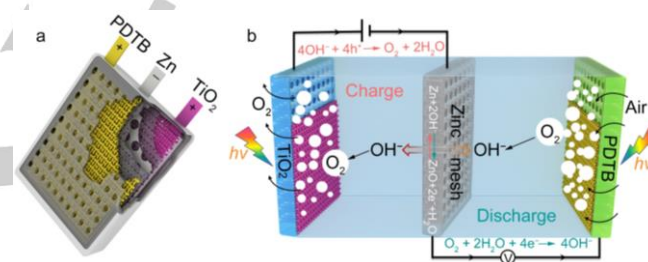


**Figure 1.** (a) Prototype of pouch cell and (b) Cross section of photo-involved Zn-air battery.

The photo-involved Zn-air battery is assembled in a pouch cell with a Zn mesh anode, two sandwiching cathodes of PDTB and TiO<sub>2</sub>, and electrolyte of 6.0 M KOH, as shown in **Figure 1a**. Two glass-fiber separators are used as interlayers to avoid short circuit, and uniform holes are drilled on each side of the transparent pouch cell, which allow air breath and light capture during battery operation. In a discharging process, the PDTB cathode is excited for ORR to couple with the Zn anode, breathing in O<sub>2</sub> from air; in a reverse process, the TiO<sub>2</sub> cathode is switched to light for OER, releasing O<sub>2</sub> into air, as depicted in **Figure 1b**. The two cathodes guarantee full utilization of light for the respective ORR and OER.

The monomer of (1,4-di(2-thienyl))benzene (DTB) was synthesized via Suzuki-Miyaura coupling<sup>[11]</sup> and confirmed by Raman spectroscopy in **Figure 2a** and nuclear magnetic resonance (NMR) in **Figure S1**. It was then dropped onto carbon papers for the PDTB cathode via iodine-vapor-assisted polymerization. The two characteristic peaks at 1455 and 1190 cm<sup>-1</sup> are assigned to the respective ring stretching of C<sub>α</sub>=C<sub>β</sub> and C<sub>α</sub>(C<sub>α'</sub>)-C(phenyl) in **Figure 2a** and **b**, suggesting polymerization of DTB. It was further confirmed by Fourier-transform infrared (FTIR) in **Figure S2**. The PDTB is mainly consisted of DTB dimers bonded via the C<sub>α</sub> positions with molecular weight of 482.2 from the matrix-assisted laser desorption/ionization time-of-flight (MALDI-TOF) mass spectroscopy in **Figure 2b**. The carbon fibers are evenly covered by PDTB with thickness of 50~100 nm in the scanning electron microscopy (SEM) images

[\*] D. Du, S. Zhao, Z. Zhu, Prof. F. Li, Prof. J. Chen  
Key Laboratory of Advanced Energy Materials Chemistry (Ministry of Education), Renewable Energy Conversion and Storage Center (RECAST), College of Chemistry, Nankai University, Tianjin 300071, China  
E-mail: fujunli@nankai.edu.cn

Supporting information for this article is given via a link at the end of the document.

of Figure 2c and Figure S3. High-resolution transmission electron microscopy (TEM) images in Figure S4 and X-ray diffraction (XRD) patterns in Figure S5 indicate that the PDTB is crystalline, which is ascribed to the intramolecular  $\pi$ - $\pi$  stacking.

The TiO<sub>2</sub> was synthesized by seed-assisted hydrothermal method,<sup>[12]</sup> followed by sintering at 550 °C in Ar. It features as vertically aligned TiO<sub>2</sub> nanorod arrays with diameters of ~100 nm on carbon fibers in Figure 2d and Figure S6. It is rutile phase as revealed by XRD and Raman spectrum in Figure S7 and Figure S8. Well-developed lattice fringes in Figure 2e and Figure S9 suggest high crystallinity, where yellow circles indicate oxygen vacancies. The typical facet (110) of TiO<sub>2</sub> and its corresponding *d*-spacings of 0.33 nm are revealed by the selected-area electron diffraction (SAED) pattern. Furthermore, a strong signal with *g*-value of 2.003 of electron paramagnetic resonance (EPR) of TiO<sub>2</sub> in Figure 2f confirms oxygen vacancies, consistent with the TEM image in Figure 2e and XPS spectra in Figure S10.

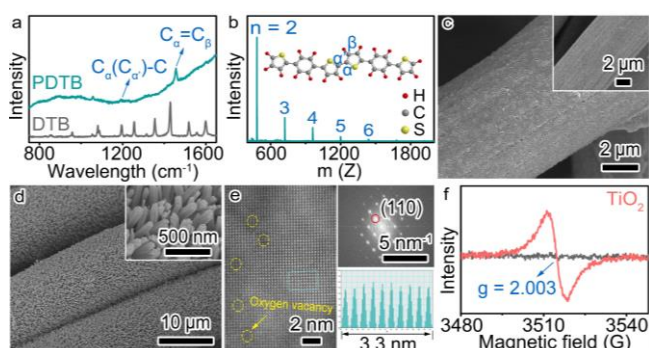


**Figure 2.** (a) Raman spectra, (b) MALDI-TOF mass spectroscopy (*n* refers to DTB unit number), and (c) SEM images of PDTB; (d) SEM images, (e) STEM, SAED pattern, and distribution of *d*-spacings of TiO<sub>2</sub>, and (f) EPR of carbon papers with and without TiO<sub>2</sub>.

**Figure 3a** presents the ultraviolet-visible (UV-vis) absorption spectroscopy of PDTB and TiO<sub>2</sub>, in which their absorption edges are revealed to be 578 and 429 nm, respectively. This corresponds to the band gaps (*E<sub>g</sub>*) of 2.14 and 2.89 eV in Figure S11. Ultraviolet photoelectron spectroscopy (UPS) in Figure 3b shows that the secondary edges of PDTB and TiO<sub>2</sub> are 16.1 and 16.3 eV, respectively, from which their work functions are derived to 5.10 and 4.90 eV by subtracted by the excitation energy of 21.2 eV. Then, the conduction band minimum edges of PDTB and TiO<sub>2</sub> are calculated to be 0.84 and 0.17 V against normal hydrogen electrode (NHE, corresponding to -4.44 eV of the vacuum energy),<sup>[13]</sup> respectively. Because the band edge varies with pH in aqueous solutions following a Nernstian relation of potential shift of ~60 mV/pH,<sup>[10,14]</sup> the estimated conduction bands (CB) of PDTB and TiO<sub>2</sub> are -0.02 and -0.69 V in 6.0 M KOH electrolyte (pH ≈ 14.4), and their corresponding valence bands (VB) are 2.12 and 2.20 V, respectively. The overall energy diagram is shown in Figure S12, in which the redox couple of O<sub>2</sub>/OH<sup>-</sup> is located between the CB and VB of both PDTB and TiO<sub>2</sub>.

Time-resolved photoluminescence (PL) spectroscopy in Figure 3c shows that the fluorescence lifetime ( $\tau$ ) of PDTB and TiO<sub>2</sub> are 5.98 and 7.38 ns, respectively, upon excitation of 474 and 460 nm. The recombination of photo-generated electron-hole pairs is limited, as shown in Figure S13. It indicates that the lifetime of charge carriers on the PDTB cathode is in the same time scale to the ubiquitous TiO<sub>2</sub> cathode.<sup>[15]</sup> A standard three-

electrode setup with the PDTB or TiO<sub>2</sub> working electrode, graphite rod counter electrode, Hg/HgO reference electrode and electrolyte of O<sub>2</sub>-concentrated 6.0 M KOH is employed to study the photo-response when exposed to 365 nm illumination (~90 mW cm<sup>-2</sup>) without applied bias voltages. It is notable that, without illumination, no current is detected on either PDTB or TiO<sub>2</sub> and Pt/C + RuO<sub>2</sub> electrode in Figure 3d and Figure S14; while upon illumination, the ORR and OER currents on PDTB and TiO<sub>2</sub> are 5.2 and 13.5 mA cm<sup>-2</sup>, respectively. These indicate that the photo-excited electrons or holes on PDTB or TiO<sub>2</sub> have long lifetimes to be efficiently transferred to the redox couple of O<sub>2</sub>/H<sub>2</sub>O for electrocatalytic ORR and OER. It agrees with the smaller interfacial charge transfer resistance under illumination than in dark, as revealed in the electrochemical impedance spectroscopy (EIS) in Figure S15. These imply that the charge carriers can be effectively separated under illumination and transferred for the respective ORR and OER on the PDTB and TiO<sub>2</sub> electrode.

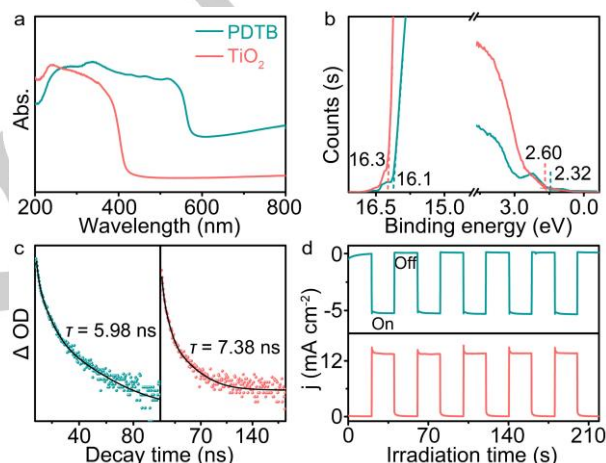


**Figure 3.** (a) UV-vis absorption spectra from 200 to 800 nm, (b) UPS measurements for VB and estimation of CB, (c) Time-resolved PL decay profiles at excitation wavelengths of 474 and 460 nm for PDTB and TiO<sub>2</sub>, respectively, and (d) Photocurrents under intermittent illumination of 365 nm without applied bias voltages on PDTB and TiO<sub>2</sub> cathodes.

To gain insights into the ORR and OER on the respective PDTB and TiO<sub>2</sub>, a three-electrode system with the electrolyte of O<sub>2</sub>-saturated 6.0 M KOH is employed. The linear sweep voltammetry (LSV) curve of PDTB for ORR in **Figure 4a** shows that its onset potential upon illumination reaches up to 1.44 V versus reversible hydrogen electrode (RHE). It is higher by 460 mV than the state-of-the-art Pt/C + RuO<sub>2</sub> and even 200 mV in comparison with the equilibrium of O<sub>2</sub>/H<sub>2</sub>O, 1.23 V. For the OER on TiO<sub>2</sub>, the illuminated onset potential is significantly reduced to 0.24 V, compared to 1.36 V on the Pt/C + RuO<sub>2</sub> in Figure 4b. Both of the operation potentials for ORR and OER on the respective PDTB and TiO<sub>2</sub> in Figure S16 are stable during the 3-hours test, regardless of irradiation. The demonstrated ORR and OER potentials off the equilibrium of O<sub>2</sub>/H<sub>2</sub>O on PDTB and TiO<sub>2</sub> are attributed to the light illumination, which are consistent with the photo-responses in Figure 3d.

The short-lived oxygen-containing intermediates in the ORR and OER processes under illumination are trapped by dimethyl pyridine N-oxide (DMPO) and then detected by EPR spin-trap technique. Figure 4c shows sextet EPR peaks in the electrolyte contacting with PDTB in the ORR process under illumination,

which is in contrast with no signals in dark. The characteristic peaks of the EPR with PDTB are assigned to the DMPO-O<sub>2</sub><sup>•-</sup> adduct, which is derived from reduction of O<sub>2</sub> by photoelectrons. In the OER process on the TiO<sub>2</sub> electrode under illumination, the DMPO-OH<sup>•</sup> adduct<sup>[16]</sup> is identified by the characteristic EPR peaks in Figure 4d, of which the OH<sup>•</sup> species is formed from OH<sup>-</sup> by accepting highly oxidative photo-generated holes. The EPR signals with both PDTB and TiO<sub>2</sub> responding to illumination are consistent with the photocurrents in Figure 3d. It is clear that the photo-generated electrons and holes on the PDTB and TiO<sub>2</sub> electrode can be effectively transferred to participate in the electrocatalytic ORR and OER with O<sub>2</sub><sup>•-</sup> and OH<sup>•</sup> as the respective intermediates.

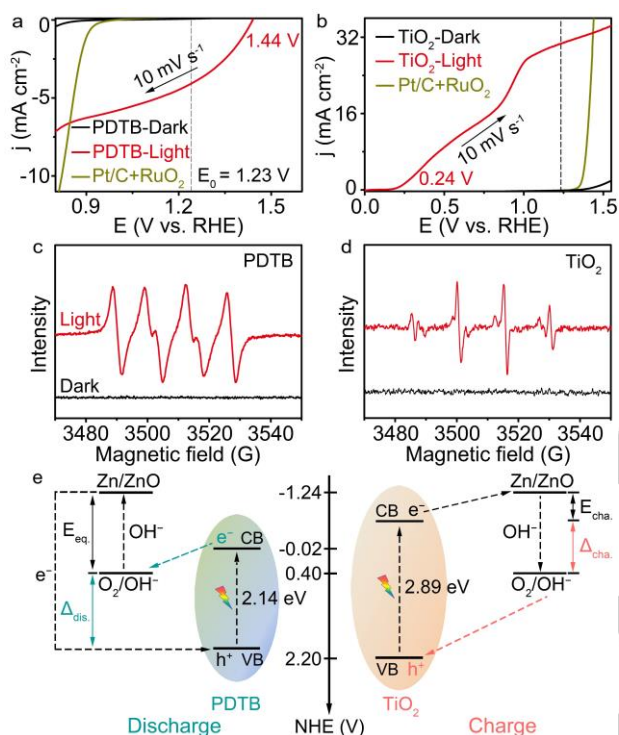
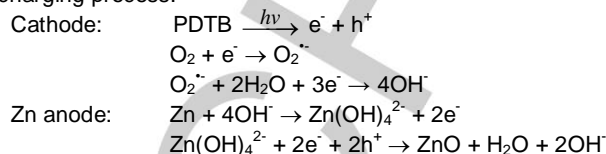


**Figure 4.** ORR polarization curves of PDTB (a) and TiO<sub>2</sub> (b) with and without illumination of 365 nm, as well as Pt/C + RuO<sub>2</sub>; EPR spectra of oxygen-containing intermediates derived on the surface of PDTB (c) and TiO<sub>2</sub> (d) with and without illumination with DMPO as a radical trapping reagent; and (e) Proposed reaction mechanism of the photo-involved Zn-air batteries.

The mechanism of photo-excited ORR and OER for Zn-air batteries is proposed in Figure 4e. In the discharging process with illumination, the PDTB cathode harvests photons and generates electron-hole couples. The photoelectrons located in the CB of PDTB are transferred to O<sub>2</sub> for its electrocatalytic reduction; at the same time, the holes left behind in the VB of PDTB are accepted by Zn for ZnO via the external circuit, which is confirmed by XRD patterns in Figure S17. The discharge voltage is defined by the VB of PDTB and the redox of Zn/ZnO, and therefore is over the equilibrium of 1.64 V due to the contribution of light, as depicted in Figure 4e and consistent with Figure 4a. In the charging process, the photo-generated holes with strong oxidation capability in the VB of TiO<sub>2</sub> are driven for the conversion of OH<sup>-</sup> to OH<sup>•</sup> by an applied voltage, which then decomposes to release O<sub>2</sub>; meanwhile, the photoelectrons are transported through the external circuit to the anode for the reduction of ZnO to Zn. The charge voltage is corresponding to the potential difference between the redox of Zn/ZnO and the

CB of TiO<sub>2</sub>, which is reduced below the equilibrium in Figure 4e and in agreement with Figure 4b. The reversible formation and decomposition of ZnO/Zn on the double sides of Zn mesh are confirmed by XRD patterns in Figure S17 and SEM images in Figure S18. The reactions at the PDTB or TiO<sub>2</sub> cathodes and Zn anode in the discharging and charging processes of the Zn-air batteries are illustrated below:

Discharging process:



Charging process:

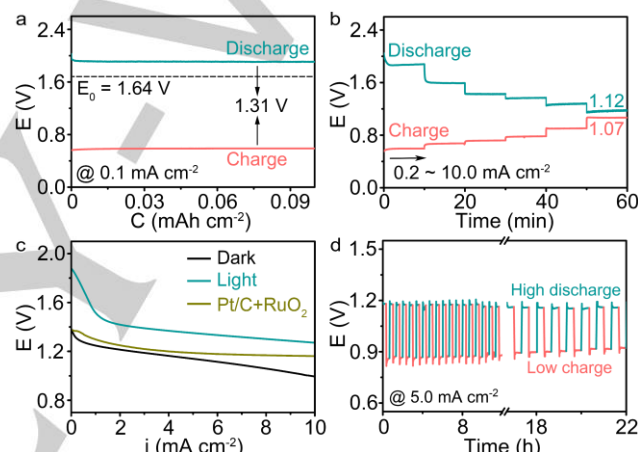
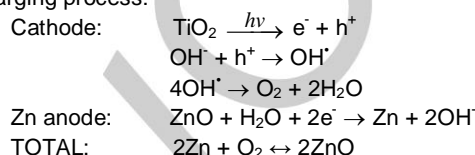


**Figure 5.** (a) Discharge/charge profiles at 0.1 mA cm<sup>-2</sup> under illumination (365 nm, 90 mW cm<sup>-2</sup>), (b) Discharge/charge profiles at current densities from 0.2 to 0.5, 1.0, 2.0, 5.0, and 10.0 mA cm<sup>-2</sup>, (c) Discharge profiles of PDTB with and without illumination at a scan rate of 0.01 mA s<sup>-1</sup>, as well as Pt/C + RuO<sub>2</sub>, (d) Cycling performance at 5.0 mA cm<sup>-2</sup>.

The photo-involved Zn-air battery is constructed in Figure 1. In a discharging process, the PDTB cathode is exposed to light and coupled with the Zn anode; in a reverse process, the TiO<sub>2</sub> cathode is switched to light. **Figure 5a** displays the discharge and charge profiles of the Zn-air battery at 0.1 mA cm<sup>-2</sup> under illumination of 90 mW cm<sup>-2</sup> with wavelength of 365 nm. The discharge voltage with the PDTB cathode reaches up to a record-high value of 1.90 V, which surpasses by 260 mV than the thermodynamic limit of 1.64 V of Zn-air batteries. Meanwhile, a record-low charge voltage of 0.59 V is achieved with the TiO<sub>2</sub> cathode, which is lower by 1.29 V than the state-of-the-art Pt/C + RuO<sub>2</sub> of 1.88 V in Figure S19. The sensitive behaviors of the Zn-air battery to light are in good accordance with the ORR and OER processes in Figure 4a and b. Of note, the involvement of light in the Zn-air battery can significantly increase the discharge voltage and reduce the charge voltage, so that its discharge voltage is abnormally higher than its charge voltage in an empirical view. This suggests additional conversion of photo-energy to electric and chemical energy on the PDTB and TiO<sub>2</sub> cathodes of the Zn-air battery in the discharging and charging processes, respectively.

Figure 5b shows the discharge and charge profiles of Zn-air battery at varied current densities under illumination. The discharge voltage plateaus gradually decrease from 1.87 to 1.60, 1.42, 1.36, 1.26, and 1.12 V, and the charge voltage increases from 0.61 to 0.67, 0.72, 0.78, 0.90, and 1.07 V, as the current density is changed from 0.2 to 0.5, 1.0, 2.0, 5.0, and 10 mA cm<sup>-2</sup>. The discharge voltages remain higher than the charge voltages, though the voltage difference between discharge and charge is reducing. This counterintuitive tendency upon illumination is in contrast to the dark condition in Figure S20 and the Zn-air battery with Pt/C + RuO<sub>2</sub> in Figure S21. The discharge voltages of the Zn-air battery under illumination at small currents below 1.0 mA cm<sup>-2</sup> are significantly higher than in dark and Pt/C + RuO<sub>2</sub> in Figure 5c. This is superior to the reported Zn-air batteries with and without illumination in Table S1. Even at the condition of AM 1.5, the discharge voltage is still higher than the charge voltage in Figure S22, both of which are sensitive to the illumination. The cycling performance of the photo-involved Zn-air battery is presented in Figure 5d, in which the discharge and charge voltages are 1.18 and 0.86 V, respectively, at 5 mA cm<sup>-2</sup>, corresponding to energy efficiency of 48.1% considering the light energy. It displays good cycle stability, as also evidenced by the stable cathodes of PDTB and TiO<sub>2</sub> in Figure S23 and S24 and the reversible cathode reactions in the XRD pattern in Figure S17, respectively. It is in contrast to the big polarization of 0.84 V in the Zn-air battery with Pt/C + RuO<sub>2</sub> in Figure S25. Although the contribution of light to the discharge and charge voltages is significant from 0.1 to 10 mA cm<sup>-2</sup>, it would be reduced as the current is largely increased. This is related to the compatibility of the lifetimes of photo-excited charge carriers in the semiconducting electrode with its interfacial charge transfer for ORR and OER. It is believed that the power density of the photo-involved Zn-air battery and its incident photon-to-current efficiency (IPCE, Table S2) can be largely enhanced by the rationally-designed semiconducting materials and its tunable microstructures.

In conclusion, a photo-involved Zn-air battery with two semiconducting PDTB and TiO<sub>2</sub> cathodes to sandwich a Zn anode is constructed to harvest light energy. The PDTB and TiO<sub>2</sub> are sensitive to light illumination to allow separation of electrons and holes, the lifetimes of which are compatible with the interfacial charge transfer for the electrocatalytic ORR and OER, respectively. In the discharging process, the photoelectrons in the CB of PDTB are donated to O<sub>2</sub> for its reduction to O<sub>2</sub><sup>•-</sup> that then converts to OH<sup>-</sup>, and the holes left behind in the VB are transferred for oxidation of Zn to ZnO. In the reverse process on TiO<sub>2</sub>, the holes are driven by an applied voltage for oxidation of OH<sup>-</sup> to OH<sup>•</sup>, and then it decomposes to release O<sub>2</sub>. An unprecedented discharge voltage of 1.90 V and charge voltage of 0.59 V are obtained in the photo-involved Zn-air battery. This is related to the additional light contribution, which can be converted to electric energy in the discharging process and chemical energy in the charging process.

## Acknowledgements

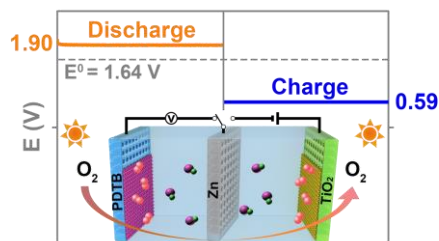
Financial support from National Natural Science Foundation of China (grant No., 21822506, 51761165025, and 51671107), National Key R&D Program of China (2017YFA0206700), and the 111 project of B12015 is acknowledged.

## Conflict of interest

The authors declare no conflict of interest.

**Keywords:** Zn-air batteries • oxygen reduction reactions • oxygen evolution reactions • output voltage • charge carrier

- [1] a) Y. Li, H. Dai, *Chem. Soc. Rev.* **2014**, *43*, 5257-5275; b) J. Lee, S. Kim, R. Cao, N. Choi, M. Liu, K. Lee, J. Cho, *Adv. Energy Mater.* **2011**, *1*, 34-50.
- [2] Q. Zhao, Z. Yan, C. Chen, J. Chen, *Chem. Rev.* **2017**, *117*, 10121-10211.
- [3] a) Z. Zhao, X. Fan, J. Ding, W. Hu, C. Zhong, J. Lu, *ACS Energy Lett.* **2019**, *4*, 2259-2270; b) F. Li, J. Chen, *Adv. Energy Mater.* **2017**, *7*, 1602934.
- [4] a) C. Li, X. Han, F. Cheng, Y. Hu, C. Chen, J. Chen, *Nat. Commun.* **2015**, *6*, 7345; b) Z. Zhu, X. Shi, D. Zhu, L. Wang, K. Lei, F. Li, *Research* **2019**, 6180615.
- [5] a) D. Schmidt, M. Hager, U. Schubert, *Adv. Energy Mater.* **2016**, *6*, 1500369; b) Y. Pu, G. Wang, K. Chang, Y. Ling, Y. Lin, B. Fu, C. Liu, X. Lu, Y. Tong, J. Zhang, Y. Hsu, Y. Li, *Nano Lett.* **2013**, *13*, 3817-3823; c) M. Yu, X. Ren, L. Ma, Y. Wu, *Nat. Commun.* **2014**, *5*, 5111; d) J. Lv, Y. Tan, J. Xie, R. Yang, M. Yu, S. Sun, M. Li, D. Yuan, Y. Wang, *Angew. Chem. Int. Ed.* **2018**, *57*, 12716-12720; e) Y. Liu, N. Li, S. Wu, K. Liao, K. Zhu, J. Yi, H. Zhou, *Energy Environ. Sci.* **2015**, *8*, 2664-2667; f) X. Yang, X. Feng, X. Jin, M. Shao, B. Yan, J. Yan, Y. Zhang, X. Zhang, *Angew. Chem. Int. Ed.* **2019**, *58*, 16411-16415.
- [6] K. Sivula, R. De Krol, *Nat. Rev. Mater.* **2016**, *1*, 15010-15025.
- [7] B. Zhang, S. Wang, W. Fan, W. Ma, Z. Liang, J. Shi, S. Liao, C. Li, *Angew. Chem. Int. Ed.* **2016**, *55*, 14748-14751.
- [8] Z. Zhu, X. Shi, G. Fan, F. Li, J. Chen, *Angew. Chem. Int. Ed.* **2019**, *58*, 19021.
- [9] a) Z. Fang, Y. Zhang, X. Hu, X. Fu, L. Dai, D. Yu, *Angew. Chem. Int. Ed.* **2019**, *58*, 9248-9253; b) D. Zhu, Q. Zhao, G. Fan, S. Zhao, L. Wang, F. Li, J. Chen, *Angew. Chem. Int. Ed.* **2019**, *58*, 12460; c) A. Gurung, Q. Qiao, *Joule* **2018**, *2*, 1217-1230.
- [10] X. Liu, Y. Yuan, J. Liu, B. Liu, X. Chen, J. Ding, X. Han, Y. Deng, C. Zhong, W. Hu, *Nat. Commun.* **2019**, *10*, 1-10.
- [11] K. Oka, K. Noguchi, T. Suga, H. Nishide, B. Wintherjensen, *Adv. Energy Mater.* **2019**, *9*, 1803286.
- [12] Q. Liu, J. Xu, D. Xu, X. Zhang, *Nat. Commun.* **2015**, *6*, 7892-7899.
- [13] G. Xiao, X. Wang, D. Li, X. Fu, *J. Photochem. Photobiol. A: Chem.* **2008**, *193*, 213-221.
- [14] Y. Matsumoto, T. Yoshikawa, E. Sato, *J. Electrochem. Soc.* **1989**, *136*, 1389-1391.
- [15] a) A. Imanishi, T. Okamura, N. Ohashi, R. Nakamura, Y. Nakato, *J. Am. Chem. Soc.* **2007**, *129*, 11569-11578; b) X. Song, D. He, W. Li, Z. Ke, J. Liu, C. Tang, L. Cheng, C. Jiang, Z. Wang, X. Xiao, *Angew. Chem. Int. Ed.* **2019**, *58*, 2-10.
- [16] S. Huang, Y. Xu, Q. Liu, T. Zhou, Y. Zhao, L. Jing, H. Xu, M. Li, *Appl. Catal. B: Environ.* **2017**, *218*, 174-185.



Dongfeng Du, Shuo Zhao, Zhuo Zhu, Fujun Li\*, and Jun Chen

Page No. – Page No.

**Photo-excited oxygen reduction and oxygen evolution reactions enabling a high-performance Zn-air battery**

A novel photo-involved Zn-air battery with two semiconducting PDTB and TiO<sub>2</sub> cathodes sandwiching a Zn anode is constructed, which is enabled by photo-excited ORR and OER in the discharging and charging processes, respectively. The resultant discharge voltage of 1.90 V is much higher than the charge voltage of 0.59 V, due to the contribution of photo-energy.